A FLUID INCLUSION AND STABLE-ISOTOPE STUDY OF HYDROTHERMAL VEIN MINERALIZATION, SCHWARZWALD DISTRICT, GERMANY

Baatartsogt Baldorj[1], Thomas Wagner[2], Gregor Markl[2]*

[1]*The Nuclear Energy Comission,Executive office, Ulaanbaatar, Mongolia*
[2]*University of Tuebingen, Germany*

ABSTRACT

A combined fluid inclusion and stable isotope study has been carried out on over 180 individual samples from 89 post-Variscan hydrothermal veins (Pb-Zn-Cu-bearing fluorite-barite-quartz veins, Co-Ni-Ag-Bi-U-bearing barite-fluorite-quartz veins and barren barite-fluorite-quartz veins) from the Schwarzwald district, Germany. The salinities of fluid inclusions in post-Variscan primary fluorite, calcite, barite and quartz are in the range of 22–25 wt.% equivalent (eqv.) NaCl, and the eutectic temperatures range between –57 and –45°C, indicating the presence of H_2O-NaCl-$CaCl_2$ fluids. Homogenization temperatures vary from 130 to 180°C. A low-salinity fluid (0 to 15 wt.% eqv. NaCl) was observed in some late stage fluorite, calcite and quartz samples, which were trapped similar temperature, range of high salinity fluids.

Raman microprobe analyses show that the only detectable volatile in the vapour is CO_2. Almost all $\delta^{18}O$ (n=86) measurements of quartz from the fluorite-bearing post-Variscan veins range between +11.1 and +20.9 ‰. The calculated $\delta^{18}O_{H2O}$ values are between –11.0 and +4.4 ‰, using known quartz-water fractionation and fluid inclusion homogenization temperatures. The $\delta^{18}O_{H2O}$ values of directly extracted fluid inclusion water of fluorites range from –11.6 to +1.1 ‰, very consistent with the calculated values. The δD values of fluid inclusion water in calcites (extracted from primary and late calcite samples) lie in a narrower range between –26 and –15 ‰. The extracted fluid inclusion water from quartz samples has significantly more variable δD values between –63 and +9 ‰. The $\delta^{13}C$ and $\delta^{18}O$ values of fluid inclusion gas (CO_2) range between –21.4 and –6.7 ‰ and between –16.3 to –7.1 ‰, respectively.

Calculations for fluorite-barite-quartz veins combining oxygen isotope equilibria with microthermometric data result in quartz precipitation temperatures of 120–170°C at pressures between 0.3 to 0.5 kbar. The $\delta^{18}O_{H2O}$ and δD data, particularly the observed wide range in hydrogen isotopic compositions, indicate that the hydrothermal mineralization formed through large-scale mixing of a basement-derived saline NaCl-$CaCl_2$ brine with meteoric water.

Keywords: Schwarzwald, fluid inclusion, Variscan, viens, quartz

*corresponding author e_mail address: b_btr@yahoo.com

1. Introduction

Mesozoic hydrothermal activity and mineralization related to the initial opening of the north Atlantic ocean were first identified by Mitchell & Halliday (1976). This mineralization is characterized by base metals (mostly Pb-Zn) with minor amounts of Ag, which are hosted in quartz-carbonate-fluorite-barite veins. It has been noted that these base-metal veins occur preferentially along the margins of Mesozoic basins, particularly in the vicinity of older granites (Mitchell & Halliday 1976; Halliday & Mitchell 1984). The fluids are typically $CaCl_2$-NaCl-rich brines of moderate to high salinity with homogenization temperatures in the range 70-200°C. Features indicative of repeated mixing with cooler meteoric waters, e.g. alternating growth zones within gangue minerals hosting high- and low-salinity fluid inclusions, are very abundant (Lüders & Franzke 1993). Pronounced examples of this widespread mineralization style are found in the French Massif Central (Munoz *et al*. 1994; 2005), the Paris basin (Charef & Sheppard 1988; Clauer *et al*. 1995), southwest Cornwall (Gleeson *et al*. 2000), Ireland (Wilkinson *et al*. 1995; 1999), Spain (Canals & Cardellach 1993) and many areas in Germany (Behr *et al*. 1987; Behr & Gerler 1987; Franzke *et al*. 1996; Meyer *et al*. 2000).

The Schwarzwald district is one of the classic mining regions in Germany and well known for Pb-Zn-Ag mineralization that occurs in hydrothermal fluorite-barite-calcite-quartz veins in the Variscan crystalline basement. The mining potential of the Schwarzwald can be estimated as 0.2-0.3 Mt of Pb+Zn (Walther 1981); the fluorite+barite resources are on the order of about 10 Mt (Huck & Walther 1984). Based on fluid inclusion characteristics the hydrothermal veins in the Paleozoic basement and Permian-Mesozoic cover rocks of Germany can be grouped into two main classes (Behr & Gerler 1987), which are (1) mineralizations geologically and structurally related to the Variscan metamorphism and deformation or to Paleozoic granitic intrusions, and (2) mineralizations related to post-Variscan tectonic processes, such as the rifting of the northern Atlantic ocean in the Jurassic-Cretaceous. In contract, post-Variscan vein mineralizations with barite, fluorite and Pb-Zn ores contain fluid inclusions of the H_2O-NaCl-$CaCl_2$ type, which have high salinities (21-26 wt.% equivalent NaCl) and homogenization temperatures in a much narrower range of 150-200°C (Behr & Gerler 1987). These post-Variscan fluids were most likely derived from formation waters that migrated out of Permo-Triassic sedimentary basins into the Variscan basement. Fluid-rock interaction at temperatures of 300-350°C resulted in leaching of metals from the granites and gneisses; subsequent ascent of these metal-bearing brines along fault zones and mixing with meteoric sulphate and/or bicarbonate waters caused the hydrothermal vein mineralization (Behr & Gerler 1987).

In this paper we present fluid inclusion characteristics of post-Variscan hydrothermal veins, oxygen isotopic data of vein quartz and hydrogen, oxygen and carbon isotope analyses of inclusion fluids from a large number of hydrothermal veins covering the entire Schwarzwald district. Based on this data and calculations of isotopic fractionation trends, we establish the fluid compositions and the physico-chemical conditions of ore formation. By integrating the available information on potential fluid sources and the geological framework, we then develop a consistent model of hydrothermal mineralization in the Schwarzwald district.

2. Geology

The Schwarzwald crystalline basement complex belongs to the Moldanubian zone of the central-European Variscan orogen and covers an area of approximately 150 by 80 km in southwest Germany. In the area of the Schwarzwald numerous SSW-NNE and E-W trending shear zones of Variscan origin are widespread phenomena. The timing of the extension tectonics is well controlled by the age of the deformed Albtal granite (Rb/Sr: 326 ±2 Ma, Schuler and Steiger 1978) and the Malsburg granite (U/Pb: 328 ±6 Ma, Todt 1976). The oldest fault controlled mineralizations are scheelite (Werner *et al*.1990) and fine dispersed sulphides in cherts, which mineralised ductile-cataclastic shear zones of probably Variscan origin. The crystalline basement rocks have been exposed to the surface during the formation of the Tertiary Rheingraben structure (Kalt *et al*. 2000; Werner & Franzke 2001). The basement is predominantly composed of granitic and mafic gneisses that are locally migmatized, and post-deformational granitic plutons of moderate size. Figure 1 shows the general geology of the b asement and the major units of the post-Variscan sedimentary cover.

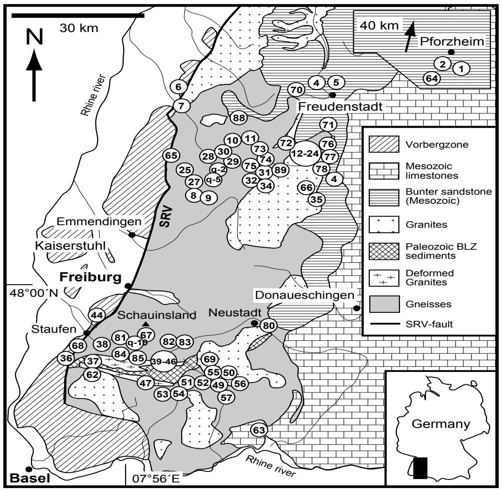

Fig. 1. Simplified geological map of the Schwarzwald showing location of the post-Variscan hydrothermal vein deposits (after Walther *et al.*1986). Numbers correspond to the Table 1.

The Schwarzwald district hosts more than 400 individual hydrothermal veins which cut the Variscan crystalline basement and the overlying sedimentary cover (Fig. 1). They have been classified into (1) quartz veins, which are most probably of Variscan origin, and (2) post-Variscan metal-bearing fluorite-barite-quartz veins. Based on their mineralogy, several sub-types of hydrothermal mineralization can be distinguished, which are, for example, Sb-Ag-bearing quartz veins (most likely Variscan, occurring throughout the entire district), Co-Ni-Ag-Bi-U-bearing barite-fluorite-veins (post-Variscan, in the Wittichen area), Fe-Mn-bearing quartz-barite-veins (Jurassic, in the Eisenbach area) and the post-Variscan to Tertiary Pb-(Zn)-(Ag)-bearing quartz-fluorite-assemblages in the southern and central Schwarzwald (Metz *et al.* 1957; Bliedtner & Martin 1988).

Most of these veins do not host minerals suitable for radiometric dating. Few measurements of uraninite (U-Pb and U-Xe, Xe-Xe), hematite (U-He), and K-bearing minerals (K-Ar) revealed three mineralization events, one at 310-280 Ma related to the end of the Variscan orogeny (Hofmann & Eikenberg 1991; Segev *et al.* 1991; Meshik *et al.* 2000). Most of the crystalline rocks show various degrees of hydrothermal alteration, with chloritization of biotite and sericitization and albitization of feldspars being the most notable alteration reactions. Entirely fresh metamorphic or igneous rocks are virtually absent in the Schwarzwald area.

3. Sampling and analytical methods

Most of the sample material used for this study was obtained in the field; additional samples were taken from private collections and the departmental collection. Samples of hydrothermal quartz, fluorite, barite and calcite from about 89 different post-Variscan hydrothermal deposits have been analyzed. The locations are shown in Fig. 1; the names and hydrothermal assemblages of the deposits are listed in Table 1. The selected deposits host various proportions of fluorite, quartz, calcite and barite as the major vein-filling gangue minerals, which are associated with complex ore assemblages. Most of the veins crosscut the gneisses and granites of the Variscan crystalline basement, but some deposits are also hosted by sedimentary rocks.

Table 1. Names of deposits and hydrothermal assemblages of post-Variscan fluorite-bearing veins; Number of deposit from figure 1.

No.	Deposit	Assemblage	No.	Deposit	Assemblage
1	Käfersteige, near Pforzheim	Fluorite-Barite Ag-Cu-Bi	45	Aitern-Süd, Schönau	Fluorite-Barite-Quartz Pb-Zn-Cu
2	Heiligenwald, near Pforzheim	Fluorite	46	Schönau	Fluorite-Quartz Pb
3	Friedenweiler, near Eisenbach	Fluorite Cu-Bi	47	Herrmann, near Görwihl	Quartz-Fluorite Pb
4	Dorothea, n. Freudenstadt	Barite-Calcite Ag-Cu	48	Riedlingen, near Kandern	Fluorite
5	Wittenweiler, n. Freudenstadt	Fluorite-Barite	49	Urberg	Quartz-Fluorite-Barite-Calcite Pb-Zn-Cu
6	Zunsweier, near Offenburg	Fluorite	50	Bildsteinfelsen, Urberg	Quartz-Fluorite-Barite-Calcite Pb-Zn-Cu-Ag
7	Ohlsbach, near Offenburg	Fluorite-Apatite-(Barite)	51	Gottes Ehre, Ruprechtgang	Quartz-Fluorite-Barite-Calcite Pb-Zn-Cu-Ag
8	Hesselbach, near Oberkirch	Fluorite Cu-(Bi)	52	Neuglück, Ruprechtgang	Quartz-Fluorite Pb
9	Ödsbach, near Oberkirch	Fluorite Cu-(Bi)	53	Schwarzwaldsegen, Ruprechtgang	Quartz-Fluorite Pb
10	Clara, near Wolfach	Barite-Fluorite Cu-Ag-Pb	54	Neue Hoffnung, Ruprechtgang	Quartz-Fluorite Pb
11	Friedrich-Christian	Fluorite-Barite-Quartz-Calcite Pb-Cu-Ag-Bi	55	Ruprechtgang, Urberg	Quartz-Fluorite Pb
12	Sophia, Wittichen	Barite-Fluorite Co-Ni-Ag-Bi-U	56	Brenden	Quartz-Fluorite Pb-(Cu)
13	Johann, Wittichen	Barite-Fluorite Bi-Cu	57	Igelschlatt, Schlüchttal	Quartz-Fluorite Pb-Cu-(Zn)
14	Neuglück, Wittichen	Barite-Fluorite Co-Ni-Ag-Bi-U	58	Hausen, Wiesental	Fluorite
15	Bleilersgrund, Wittichen	Fluorite	59	Wehratal	Fluorite
16	Ilse i. Kaltbrunn, near Wittichen	Fluorite Cu-Bi	60	Tierlen, near Witzau	Fluorite-Barite-Quartz Pb-Zn
17	Burgfelsen, Ilse, near Wittichen	Fluorite	61	Nöggenschwiel	Fluorite
18	König David, Gallenbach	Fluorite-Barite Cu-Bi-Co	62	Sulzburg	Quartz (Amethyst)

No.	Deposit	Assemblage	No.	Deposit	Assemblage
19	Hilfe Gottes, near Schiltach	Quartz Co-Bi-U	63	Mühlsteinbruch, near Waldshut	Quartz-(Barite)-(Fluorite)
20	Herzog Friedrich, Reinerzau	Fluorite-Barite Co-Ag-U	64	Neubulach	Quartz-Barite-Calcite Cu
21	Daniel Gallenbach, Wittichen	Fluorite-Barite Cu-Bi	65	Michael im Weiler	Barite Pb-Zn
22	Neubergmännisch Glück, Wittichen	Fluorite Cu-Bi	66	Geigeshalde	Barite Bi
23	Schlechthalde, near Wittichen	Fluorite	67	Schauinsland	Quartz-Barite-Calcite Pb-Zn
24	Southern Reinerzau valley	Fluorite Cu-Bi	68	Kobaltgrube	Barite-Quartz-(Fluorite) Co-(Ni)-Ag-Pb-Cu-(Zn)
25	Drey, Schnellingen	Barite-Fluorite	69	Menzenschwand	Barite-Fluorite-Quartz U-(Pb)-(Cu)
26	Barbara, Schnellingen	Barite-Fluorite Pb-Zn	70	Daniel Dehs, Bad Rippoldsau	Quartz Cu-Ag-Bi
27	Segen Gottes, Schnellingen	Barite-Fluorite Pb-Zn-Ag	71	Johann Baptist, near Rippoldsau	Quartz Cu
28	Artenberg quarry, Steinach	Quartz-Calcite-Fluorite Cu-As	72	Anton im Heubach, Schiltach, Kinzig	Barite-Fluorite Co-Ni-Ag-Bi-U
29	Erzengel Gabriel, near Hausach	Fluorite-Barite Pb	73	Bernhard, Hauserbach	Quartz-Barite-Calcite Pb-Zn-Fe
30	Laßgrund, near Hausach	Fluorite-Barite Pb	74	MariaTheresia/Hauserbach Hausach,Kinzig	Quartz-Barite-Calcite Pb-Zn-Fe
31	Wenzel, near Wolfach	Barite-Calcite Ag-Sb	75	Katharina,Trillengrund, Schiltach, Kinzig	Quartz-Barite-Calcite-(Fluorite) Pb-Zn-Cu
32	Fortuna Gelbach, near Wolf ach	Fluorite-Barite Pb-Ag	76	Rötenbach quarry, near Alpirsbach	Calcite-Dolomite Co-Bi-Ag
33	Ludwigs Trost, Kuschbach	Fluorite-Barite Fe-(Pb)-(Ag)	77	Christiana, Wittichen	Baryte-(Co)
34	Hohberg, near Wolfach	Fluorite-Barite Fe	78	Simson, Wittichen	Barite-Fluorite Co-Ni-Ag-Bi-U
35	Tennenbronn, near Schramberg	Fluorite	79	St. Josef am Silberberg,Wittichen	Barite-Fluorite Co-Ni-Ag-Bi-U
36	Badenweiler	Quartz-Barite-Fluorite Pb-(Zn)-(Cu)	80	Hammereisenbach, E Titisee-Neustadt	Barite Fe-Mn
37	Sulzburg	Fluorite	81	Giftgrube,Kaltwasser, Münstertal	Dolomite-Calcite Pb-As
38	Bad Sulzburg	Quartz-Fluorite	82	Fahl, near Todtnau	Fluorite-Barite-Quartz-Pb
39	Schlossberg-W, Rammelsbach	Quartz-Fluorite-Barite Pb-Cu	83	Gschwend, near Todtnau	Fluorite-Barite Pb

No.	Deposit	Assemblage	No.	Deposit	Assemblage
40	Teufelsgrund, Münstertal	Quartz-Fluorite Pb-Ag-Zn	84	Herrenwald, Mulden valley	Fluorite-Barite-Pb-Zn
41	Tannenboden, Wieden	Fluorite-Barite-Quartz Pb-(Zn)-(Cu)-(As)	85	Anton, Wieden	Fluorite-Barite-Pb-Zn-Ag
42	Baumhalde, Todtnau	Quartz-Fluorite Pb-Ag-Zn	86	Silbergründle	Quartz-Pb
43	Brandenberg	Quartz-Fluorite-(Calcite) Pb-(Ag)-(Zn)-(Cu)	87	Königswart	Quartz-Barite-Cu-Bi
44	Schönenberg, Schönau	Fluorite-Barite-Quartz Pb-Cu	88	Silberbrünnle	Quartz-Cu
			89	Lorenz	Quartz-Cu

3.1Microthermometry and Raman spectroscopy

More than 135 individual samples from about 60 selected deposits representing 2 different hydrothermal vein types (Pb-Zn-Cu-bearing fluorite-barite-quartz veins and Co-Ni-Ag-Bi-U-bearing barite-fluorite-quartz veins) were studied by conventional fluid inclusion techniques.

Microthermometric measurements were carried out on doubly polished sections (200-400 μm thickness) using a Leica DMLP microscope equipped with a Linkam THMS-600 programmable cooling-heating stage and a digital photo camera and image analysis system. The calibration points used were the triple point of pure CO_2 (–56.6°C), the melting point of pure H_2O (0°C) and the critical homogenization of pure H_2O (374.1°C).

The reproducibility of all measured melting and homogenization temperatures is around 0.1-0.2°C and 2-3°C, respectively. Apparent salinities, expressed as weight percent (wt.%) NaCl equivalent, were calculated from the measured final ice melting temperatures of aqueous two-phase following the methods described in Roedder (1984) and Bodnar *et al.* (1994). For the system NaCl-$CaCl_2$-H_2O, salinities were termed as weight percent (wt.%) NaCl and $CaCl_2$ equivalents, thus final melting temperatures of ice and hydrohalite are required. The gas composition of the fluid inclusions of representative samples was analyzed by laser Raman spectrometry, using a Dilor LABRAM-2 Raman microspectrometer with a 514.5 nm Ar-ion laser source (Burke 2000).

3.2 Stable isotope geochemistry

We have analyzed 86 quartz samples from 33 localities in the Schwarzwald for their oxygen isotope compositions; the sample descriptions are listed in Table 3. Mineral separates were prepared by careful hand-picking under a binocular microscope, followed by cleaning in deionized water. Oxygen isotope analysis was performed using a laser extraction procedure that essentially follows the techniques described by Sharp (1990) and Rumble & Hoering (1994). Approximately 2 mg of quartz grains were loaded onto a small Pt sample holder and evacuated. After prefluorination of the sample chamber overnight, the samples were heated with a CO_2 laser at a F_2 pressure of 50 mbar. Excess F_2 was removed from the oxygen by reaction with KCl at 150°C; residual Cl_2 was separated from the oxygen using a liquid nitrogen cold trap. The extracted O_2 was collected on a molecular sieve, subsequently expanded and measured on a Finnigan MAT-252 gas source mass spectrometer for the $^{18}O/^{16}O$ isotope ratio. Reproducibility of the analytical results, and mass spectrometer calibration, was monitored through replicate measurements of the international standard NBS-28 ($\delta^{18}O_{V\text{-}SMOW}$: +9.6 ‰). The analytical precision (1σ) was around ± 0.2 ‰. All oxygen isotopic data are reported in standard delta notation, relative to V-SMOW.

Following microthermometric characterization, exclusively samples containing a single generation of fluid inclusions were selected for δD,$\delta^{18}O$ and $\delta^{13}C$ analyses of inclusion fluids in pure fluorite, quartz and calcite. Approximately 4 g of each sample having a grain size of 3-6 mm were carefully hand-picked and cleaned in deionized water. Extraction of the inclusion fluids was performed in a vacuum extraction line following techniques outlined by Kishima & Sakai (1980), Friedman (1953), Craig (1961) and Jenkin *et al*. (1994).

The samples were loaded into vacuum glass tubes and heated at 150 °C overnight. Inclusion fluids were extracted by thermal decrepitation under vacuum at 400°C for analysis of δD (fluorite, quartz, calcite), and at 650°C for analysis of $\delta^{13}C$ and $\delta^{18}O$ (only fluorite). The extracted fluids were collected in a liquid nitrogen cold trap; volatiles were not passed over a CuO furnace. The liquid nitrogen cold trap was then replaced by an alcohol and dry-ice slush (–80°C) to separate molecular water from the condensable gases (Vennemann & O'Neil 1993; Demeny 1995). The water itself was converted to H_2 gas by reaction with 150 mg of Zn (obtained from Indiana University, USA) in vacuum quartz-glass tubes for 15 minutes at about 500°C, as described by Craig (1961), and Friedman (1953).

For oxygen and carbon isotope analysis of fluid inclusions from fluorites, the cryogenically purified water was equilibrated with a measured amount of carbon dioxide gas of known initial isotopic compositions ($\delta^{13}C$ = –30.2 ‰ V-PDB, $\delta^{18}O$ = –1.07 ‰ V-PDB) for three days in a glass tube at 25°C. After equilibration, the carbon dioxide gas was separated from the water using a liquid nitrogen trap. Cryogenically purified CO_2 of inclusion gas from fluorites was directly collected. The δD and $\delta^{18}O$ values of the released fluid inclusion water and the $\delta^{13}C$ and $\delta^{18}O$ values of the released CO_2-fluid inclusion gas were measured on a Finnigan MAT-252 mass spectrometer with working standards calibrated against international standards (V-SMOW for oxygen and hydrogen, V-PDB for carbon). Results of hydrogen isotope analysis are normalized to an internal biotite and kaolinite standards, which have a δD value of –64 ±5.0 ‰ and -125 ±5.0 ‰ respectively. These internal biotite and kaolinite standards were previously calibrated against the international biotite standard NBS-30 (δD: –65 ‰).

The extraction procedure for the biotite standard was slightly different from the method described above. Biotite was heated to about 1200°C and the released volatiles were passed over a CuO furnace to oxidize hydrogen to water. The analytical precision is estimated to be better than 0.3 ‰ for oxygen and carbon, and better than 5 ‰ for hydrogen isotope compositions. Results are reported in standard delta notation, relative to V-SMOW and V-PDB.

3.3 Fluid inclusion petrography

Fluid inclusions were studied in quartz, fluorite, calcite and barite crystals representing different mineral generations. The size of the inclusions generally ranges from 5 to 40 µm, with most inclusions being about 10-20 µm in size; fluid inclusions in quartz are generally smaller, about 5-10 µm. The majorities of the fluid inclusions appear to be secondary and occur randomly distributed through the quartz, fluorite, calcite and barite crystals. The inclusions in fluorite are mostly present as clusters (Fig. 2A), as isolated inclusions (Fig. 2B), and oriented along microfractures (Fig. 2C; 2D). The inclusions are up to 40 µm in size and show mainly round, elongate, and, less commonly, irregular shapes.

Many of the fluid inclusions in barite and calcite appear to have decrepitated. Shape and occurrence of inclusions in barite and calcite are similar to the inclusions in fluorite, but the maximum sizes are less than 100 µm. Fluid inclusions in quartz are generally smaller than in the other minerals and show frequently irregular shapes; single-phase liquid aqueous inclusions are fairly abundant.

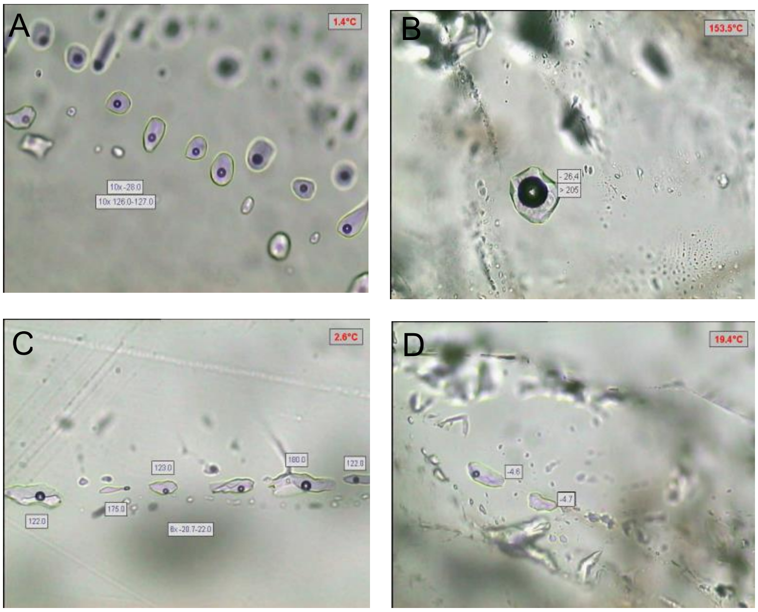

Fig. 2. Photomicrographs showing fluid inclusion types in stage I and II fluorites of post-Variscan hydrothermal deposits, Schwarzwald. **(A)**. Type 1 fluid inclusions at 1.4°C. **(B)**. Isolated type 1 fluid inclusion with lower degree of fill (CO_2). **(C)**. Type 1 fluid inclusions along the trail at 2.5°C. **(D)**. Monophase type 2 fluid inclusions with type 1 inclusions in stage II fluorite at 19°C.

According to their salinity, textural distribution and phase relationships at room temperature, three distinct types of inclusions have been distinguished, which are described below in order of decreasing abundance:

Type1 (high salinity two-phase aqueous fluid inclusions). These inclusions consist of two phases (H_2O-rich liquid + vapor), with generally higher degree of fill, $V_{liquid}/(V_{liquid}+V_{vapor})$ of about 0.9 to 0.95 and greater size. Few fluid inclusions of this type contain a single daughter crystal, most likely halite. Approximately 90 percent of all individual samples contain type 1 inclusions. There are also some fluid inclusions consist of two phases (Vapor + H_2O-liquid), with significantly lower degrees of fill, $V_{liquid}/(V_{liquid}+V_{vapor})$ generally below 0.7.

Type 2 (low salinity two-phase aqueous fluid inclusions). Aqueous inclusions of low-moderate salinity found in quartz and some late-stage fluorite samples. These inclusions consist of two phases (H_2O+ vapor), with higher degree of fill.

Type 3 (monophase fluid inclusion). This type contains only one homogeneous aqueous fluid phase, and is generally associated with type 1 inclusions.

Microthermometry

Based on the measured range in salinities, all type of fluid inclusions can be subdivided into two distinct groups.

Type 1. High-salinity aqueous fluid inclusions.

Generally, a consistent sequence of phase transitions was observed, comprising initial melting of ice, final melting of ice, final melting of hydrohalite (not clearly visible in all inclusions) and total homogenization. Initial ice melting temperatures in aqueous inclusions are in the range of –57 to –45 °C, which correspond well to the eutectic temperature of the ternary H_2O-NaCl-$CaCl_2$ system at –52 °C (Borisenko 1977). In this type of aqueous fluid inclusions, the final melting temperatures of ice range from –28 to –20 °C, which corresponds to salinities of 22.4 to 24.7 wt. % NaCl equivalent. The final melting of hydrohalite was only observed as the last melting phase in 17 samples, with temperatures ranging from –18.5 to –7 °C. In samples where both the final melting of ice (in the temperature range of –27.5 °C to –22.0 °C) and final melting of hydrohalite (in the temperature range of –18.5 °C to –7 °C), were observed, the fluid composition can be derived from the relevant ternary H_2O-NaCl-$CaCl_2$ phase diagram (Borisenko 1977). The resulting calculated fluid compositions are in the range of 11-22 wt. % NaCl and 3-17 wt.% $CaCl_2$. The total homogenization of high salinity aqueous fluid inclusions occurred exclusively into the liquid phase. Measured homogenization temperatures show considerable variation from 90 to 200 °C, with about 80 % of the data being located a much narrower range of 100-160 °C (Figs. 3, 4; Table 2).

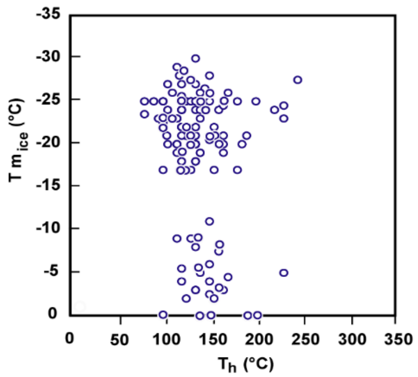

Fig. 3. T_m vs. T_h diagram for the measured fluid inclusions in fluorite bearing post-Variscan vein in Schwarzwald

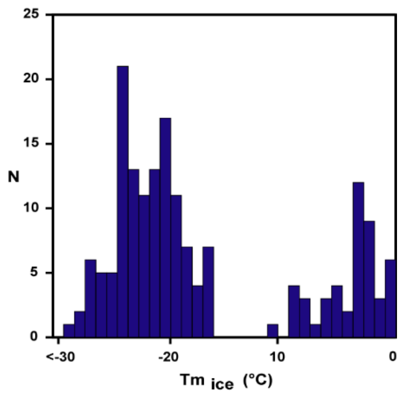

Fig. 4. Histogram showing the range of all measured ice melting temperatures (T_m) post-Variscan hydrothermal veins in the from the Schwarzwald.

Type 2. Low salinity aqueous fluid inclusion.

This fluid inclusion type is exclusively present in late-stage quartz, fluorite, and calcite samples. Only final melting of ice and total homogenization could be observed. The final ice melting temperatures range from –11.1 to 0 °C, corresponding to salinities of 0 to 15.0 wt. % NaCl equivalent. The fluid inclusions homogenize always to the liquid phase, with homogenization temperatures of between 110-200 °C. Rarely, final ice melting temperatures above 0 °C were observed, which likely indicates the presence of metastable superheated ice (Roedder 1984). Homogenization of vapour richer inclusions was observed to the liquid phase, in some cases, to the critical mode and higher homogenization temperatures were observed, 185 to 250 °C.

Type 3. Monophase Inclusions.

In monophase fluid inclusions only initial and final melting of ice could be observed. Initial ice melting temperatures are in the range of –55 to –40 °C, corresponding to the eutectic temperature of the ternary H_2O-NaCl-$CaCl_2$ system. Final melting temperatures of ice show a wide range, from –22.5 to –1.5 °C, which corresponds to salinities of 2.5 to 24.0 wt.% NaCl equivalent.

The microthermometric data obtained from the different types of fluid inclusions are summarized in Table 2. Frequency distributions of the final ice melting and homogenization temperatures for individual samples generally show a rather narrow range, indicating the presence of a comparatively homogeneous hydrothermal fluid (Fig.4). Representative fluid inclusions from the microthermometrically distinguishable groups have been analyzed with a Raman microprobe. These analyses show that CO_2 is the only detectable volatile species in the vapour phase (Fig. 5).

On a Tm-Th plot (Fig. 3) the post-Variscan inclusions display what is usually interpreted (Shepherd *et al*. 1985) as a mixing trend between fluids of different salinities but similar Th.

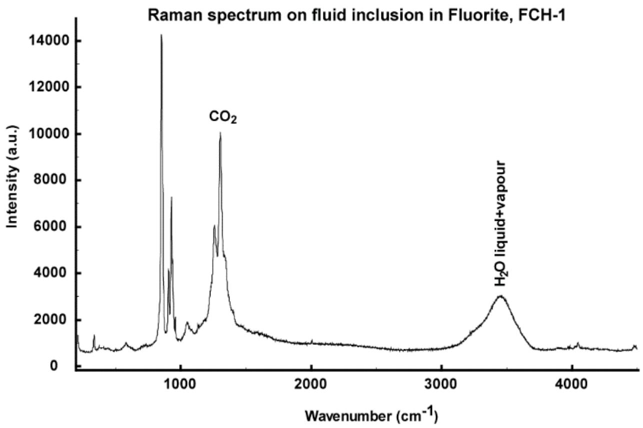

Fig. 5. Typical RAMAN spectra of fluid inclusions in fluorites. They show the dominant CO_2peak at 1285 cm^{-1} together with H_2O bands.

Table 2. Summary of Microthermometric data and compositional data of fluid inclusions from the post-Variscan hydrothermal veins of the Schwarzwald deposits.

Locality	No. of deposit	Sample	Host mineral	Type of inclusion	N	T_mHH (°C)	$T_m$ice (°C)	T_h (°C)	Salinity (wt% NaCl eq.)
Aitern Süd	45	44	Fluorite	Type 1	6		-17.2 to -16.2	111-119	19.6-20.4
				Type 2	6		-9.7 to -8.7	107-129	12.5-13.6
Artenberg	28	BTR-13	Fluorite	Type 1	97		-30.5 to -23.8	80-168	24.8-29.0
		BTR-13	Calcite	Type 1	42		-29.5 to -19.5	127-207	22.0-28.3
		XSA-15	Quartz	Type 1	11	-12.5 to -18.0	-23.5 to -22.5	50-130	24.0-24.6
		XSA-66	Calcite	Type 1	39		-28.5 to -26.5	111-165	26.5-27.7
		XSA-47	Calcite	Type 1	5		-28.7 to -26.5	93-130	26.5-27.8
		21A62	Sphalerite	Type 1	10		-36.5 to -18.5	71-117	21.2-32.9
Badenweiler	36	BTR-39	Fluorite	Type 2	40		-8.0 to -0.2	123-189	0.4-11.7
		BTR-39	Quartz	Type 2	28		-6.0 to -1.0	100-192	1.7-9.2
		BTR-38	Quartz	Type 2	7		-6.1 to -4.4	112-167	7.0-9.3
	36	41	Fluorite	Type 2	6		-3.7 to -2.1	155-184	3.5-6.0
Barbara	26	GS-196	Fluorite	Type 2	204		-3.8 to -0.1	90-140	0.2-6.2
Baumhalde	42	GS-71	Fluorite	Type 1	20		-21.2 to -19.1	107-151	21.8-23.2
				Type 2	23		-10.8 to -0.3	81-154	0.5-14.8
		GS-71	Quartz	Type 1	34		-22.8 to -15.0	114-184	18.6-24.2
		M-31	Fluorite	Type 1	44		-15.8 to -14.0	-	17.8-19.3
				Type 2	33		-8.0 to -0.3	-	0.5-11.7
Bleibach	90	249	Sphalerite	Type 1	28		-16.2 to -23.9	89-140	19.6-24.9
Brandenberg	43	GS-83	Fluorite	Type 1	104		-22.8 to -18.0	125-174	21.0-24.2
		GS-91	Fluorite	Type 1	107		-23.0 to -20.0	110-172	22.4-24.3
		GS-91	Quartz	Type 1	56		-23.4 to -15.0	90-157	18.6-24.6
		GS-99	Fluorite	Type 1	45		-22.5 to -21.0	125-170	23.0-24.0
		GS-99	Quartz	Type 1	20		-22.0 to -15.0	60-156	18.6-23.7
		GS-99	Calcite	Type 1	75		-26.8 to -19.5	100-155	22.0-26.7
		GS-100	Fluorite	Type 3	6		-19.0 to -14.0	-	17.8-21.7
		GS-111	Fluorite	Type 1	35		-21.2 to -18.8	140-167	21.5-23.2
		GS-111	Quartz	Type 1	18		-20.5 to -19.8	85-190	22.2-22.7

		001	Sphalerite	Type 1	26		-24.4 to -19.0	78-145	21.7-25.2
Brenden	56	GS-10	Fluorite	Type 1	31		-34.3 to -15.8	76-139	19.3-31.5
		GS-10	Quartz	Type 1	9		-26.0 to -15.0	71-102	18.6-26.2
		GS-15	Fluorite	Type 1	13		-23.1 to -21.8	111-134	23.6-24.4
		GS-15	Quartz	Type 1	39		-23.2 to -16.0	58-166	19.4-24.5
		GS-24	Fluorite	Type 1	109		-22.0 to -20.4	120-135	22.6-23.7
Bleilersgrund, Wittichen	15	30	Fluorite	Type 1	6		-25.9 to -20.8	70-83	22.9-26.1
Burgfelsen, Wittichen	17	14	Fluorite	Type 1	6		-23.9 to -23.0	100-101	24.3-24.9
Dorothea	4	BTR-14	Fluorite	Type 1	33	-18.8 to -17.5	-28.0 to -22.0	107-194	23.7-27.4
		QDC-52	Barite	Type 1	13	-19.5 to -17.0	-24.0 to -19.0	105-195	21.7-25.0
Drey	25	GS-151	Fluorite	Type 2	107		-3.7 to -2.7	150-170	4.5-6.0
		GS-154	Fluorite	Type 2	47		-4.6 to -2.9	122-171	4.8-7.3
Egghalde		4	Fluorite	Type 1	20		-23.3 to -21.3	110-184	23.2-24.5
Erzengel Gabriel	29	34	Fluorite	Type 2	6		-8.7 to -8.2	112-143	11.9-12.5
Friedrich-Christian	11	M-5	Calcite	Type 1	27		-29.0 to -22.1	59-115	23.8-28.0
		GS-135	Fluorite	Type 1	116		-26.8 to -21.7	109-155	23.5-26.7
		GS-135	Quartz	Type 1	30		-26.4 to -18.5	87-159	21.3-26.4
		GS-137	Fluorite	Type 1	82		-27.0 to -13.0	100-181	16.9-26.8
		FCH 1	Fluorite	Type 1	50	-20.3	-27.9 to -25.3	126-158	25.8-27.4
		FCH-2	Fluorite	Type 1	55	-21.0 to -19.0	-27.5 to -25.2	120-141	25.7-27.1
Fortuna, Wolfach	32	37	Fluorite	Type 2	21		-5.3 to -1.2	110-161	2.1-8.3
Friedenweiler, Eisenbach	3	48	Fluorite	Type 1	6		-26.1 to -13.3	162-198	17.2-26.3
Gottesehre, Urberg	51	10	Fluorite	Type 1	5		-28.0 to -27.0	131-162	26.8-27.4
		BI-26	Sphalerite	Type 2	8		-6.6 to -4.8	134-149	7.6-10.0
Hausen im Wiesental	58	9	Fluorite	Type 2	4		-5.1 to -2.8	153-164	4.6-8.0
Heiligenwald, Pforzheim	2	11	Fluorite	Type 1	5		-30.0 to -28.8	134-137	27.9-28.7
				Type 2	4		-9.0 to -8.7	129-137	12.5-12.8
Herrmann	47	M-831	Fluorite	Type 1	21		-20.9 to -8.4	105-149	12.2-23.0
		GS-67	Fluorite	Type 1	81		-20.5 to -15.0	-	18.6-22.7
		GS-68	Fluorite	Type 1	46		-25.9 to -18.8	98-176	21.5-26.1
Herzog Friedrich	20	24	Fluorite	Type 1	6		-23.7 to -19.3	90-119	21.9-24.8
Hesselbach	8	31	Fluorite	Type 1	7		-24.9 to -16.9	143-171	20.1-25.5
		7	Fluorite	Type 1	7		-26.2 to -15.5	54-96	19.0-26.3
Hohberg, Wolfach	34	23	Fluorite	Type 1	6		-26.5 to -24.0	134-154	25.0-26.5
Igelschlatt	57	GS-37	Fluorite	Type 1	71		-23.8 to -20.2	136-165	22.5-24.8

		GS-37	Quartz	Type 1	19		-34.3 to -16.9	92-143	20.1-31.5
		GS-42	Fluorite	Type 1	76		-23.4 to -16.4	70-202	19.8-24.6
Ilse im Kaltbrunn	16	5	Fluorite	Type 1	6		-26.0 to -25.4	92	25.8-26.2
Johannes, Wittichen	13	WJB-2	Fluorite	Type 1	41	-18.7 to -12.4	-25.5 to -20.0	110-173	22.4-25.9
		WJB-2	Barite	Type 1	9		-25.0 to -23.5	115-175	24.6-25.6
		WJB-4	Fluorite	Type 1	27	-18.0 to -14.6	-24.7 to -19.7	94-169	22.2-25.4
		WJB-17	Quartz	Type 1	41	-19.5 to -18.5	-31.0 to -21.0	47-125	23.0-29.3
Käfersteige	1	BTR-29	Fluorite	Type 1	82		-22.0 to -18.0	120-180	21.0-23.7
		BTR-28	Fluorite	Type 1	79		-21.0 to -19.7	99-185	22.2-23.0
Königswart	87	SW-23	Quartz	Type 1	21		-28.9 to -23.7	93-149	24.8-28.0
König David, Gallenbach	18	6	Fluorite	Type 1	6		-25.4 to -20.0	112-131	22.4-25.8
Lassgrund, Hausach	30	20	Fluorite	Type 2	6		-11.3 to -10.6	150-152	14.6-15.3
Ludwigs Trost	33	33	Fluorite	Type 2	6		-9.5 to -7.4	135-146	11.0-13.4
		45	Fluorite	Type 1	6		-25.7 to -25.0	130-145	25.6-26.0
Michael im Weiler	65	GMW-121	Quartz	Type 2	11		-6.5 to -1.5	89-130	2.6-9.9
Mühlsteinbruch	63	26	Fluorite	Type 2	6		-3.7 to -0.6	124-136	1.1-6.0
Neubergmännisch Glück	22	35	Fluorite	Type 1	6		-25.7 to -20.5	132-145	22.7-26.0
Neubulach	64	BTR-32	Quartz	Type 1	41		-27.7 to -25.0	83-140	25.6-27.2
Neuglück, Wittichen	14	BTR-37	Fluorite	Type 1	38	-15.0 to -18.5	-23.0 to -20.3	94-109	22.6-24.3
		BTR-37	Quartz	Type 3	9		-23.0 to -21.5	-	23.3-24.3
Nöggenschwiel	61	16	Fluorite	Type 1	6		-27.0 to -26.5	102-123	26.5-26.8
Ohlsbach	7	2	Fluorite	Type 1	6		-18.6 to -18.1	110-163	21.1-21.4
Ödsbach	9	8	Fluorite	Type 1	7		-17.6 to -16.4	111-198	19.8-20.7
Riedlingen	48	19	Fluorite	Type 1	5		-27.4 to -24.5	74-89	25.3-27.0
Ruprechtgangzug	52	GS-27	Fluorite	Type 1	73		-23.0 to -17.5	100-130	20.6-24.3
		GS-29b	Fluorite	Type 1	30		-21.1 to -11.5	123-198	15.5-23.1
				Type 2	9		-3.9 to -0.1	117-142	0.2-6.3
		GS-35a	Quartz	Type 1	103		-22.5 to -15.2	70-175	18.8-24.0
		GS-36a	Fluorite	Type 1	16		-22.3 to -20.6	147-166	22.8-23.9
		GS-36a	Quartz	Type 1	7		-23.8 to -20.6	112-140	22.8-24.8
Schauinsland	67	BTR-40	Quartz	Type 1	34		-24.3 to -16.0	93-155	19.4-25.1
				Type 2	16		-10.5 to -8.5	85-185	12.3-14.5
		BTR-40	Calcite	Type 1	27		-24.2 to -24.0	100-160	25.0-25.1
		364	Sphalerite	Type 1	5		-26.2 to -20.9	108-125	23.0-26.3
Schlechthalde, Wittichen	23	36	Fluorite	Type 1	6		-17.0 to -15.3	100-107	18.9-20.2

Schönau	46	32	Fluorite	Type 1	6		-22.3 to -21.1	133-152	23.1-23.9
Segen Gottes	27	56	Fluorite-late	Type 2	22		-5.8 to -0.1	88-180	0.2-8.9
		XSG-15	Fluorite	Type 2	23		-7.3 to -0.5	116-205	0.9-10.9
		BTR-47	Quartz	Type 2	26		-3.5 to -0.7	120-168	1.2-5.7
		419	Sphalerite	Type 2	4		-5.2 to -4.3	143-147	6.9-8.1
Silberbrünnle	88	BTR-31	Quartz	Type 1	44		-26.0 to -24.0	100-150	25.0-26.2
Silbergründle, Seebach	86	SW-24	Quartz	Type 1	18		-27.7 to -22.0	104-137	23.7-27.2
Sophia, Wittichen	12	BTR-17	Fluorite	Type 1	16	-23.0 to -18.5	-26.6 to -24.0	78-123	25.0-26.6
		BTR-41	Quartz	Type 1	22		-27.0 to -20.6	60-142	22.8-26.8
		BTR-41	Barite	Type 1	22		-27.0 to -24.6	100-180	25.3-26.8
		M-207	Fluorite	Type 1	52	-19.2 to -15.5	-25.0 to -22.2	80-180	23.8-25.6
		WSB-13	Quartz	Type 1	13		-24.5 to -19.4	55-132	22.0-25.3
				Type 3	5		-19.7 to -19.4	-	22.0-22.2
Sulzburg	62	13	Fluorite	Type 1	6		-20.5 to -19.8	121-146	22.2-22.7
		SW-25a	Quartz	Type 1	22		-26.8 to -22.9	81-168	24.3-26.7
		SW-25m	Quartz	Type 1	13		-24.3 to -19.2	84-139	21.8-25.1
Tannenboden, Wieden	41	38	Fluorite	Type 1	6		-20.9 to -17.6	124-176	20.7-23.0
				Type 2	4		-7.8 to -5.6	120-166	8.7-11.5
Tennenbronn	35	28	Fluorite	Type 1	6		-25.0 to -24.7	141-150	25.4-25.6
		YOB-11	Fluorite	Type 1	6		-20.9 to -19.3	138-176	21.9-23.0
Teufelsgrund	40	BTR-4	Fluorite	Type 1	36	-17.5 to -15.5	-	93-165	-
		BTR-6	Quartz	Type 1	11		-25.0 to -19.7	106-160	22.2-25.6
				Type 2	20		-11.6 to -4.9	112-207	7.7-15.6
		BTR-7	Fluorite	Type 1	30		-22.8 to -17.4	120-200	20.5-24.2
		BTR-7	Quartz	Type 1	38		-22.7 to -18.2	86-185	21.1-24.1
		BTR-9	Fluorite-late	Type 2	38		-8.6 to -3.8	124-190	6.2-12.4
		MKB-4	Sphalerite	Type 2	2		-6.8 to -5.6	118-122	8.7-10.2
Wehratal, Nöggenschwiel	59	15	Fluorite	Type 1	6		-18.9 to -17.0	123-145	20.2-21.6
Wenzel	31	49	Fluorite	Type 1	6		-28.4 to -25.9	114-139	26.1-27.7
		BTR-18	Calcite	Type 1	31		-28.9 to -27.0	100-155	26.8-28.0
		BTR-42	Calcite	Type 1	22		-28.0 to -26.5	113-160	26.5-27.4
Wildtal	91	770	Sphalerite	Type 1	30		-25.4 to -18.4	78-144	21.3-25.8
Wittenweiler	5	1	Fluorite	Type 1	5		-25.3 to -17.3	127-137	20.4-25.8
Zunsweier	6	12	Fluorite	Type 1	26		-28.4 to -18.6	132-194	21.4-27.7

4. Stable isotope characteristics

4.1Oxygen isotope data of vein quartz

The results of the oxygen isotope analyses are summarized in Table 3. All δ^{18}O values of quartz of the fluorite-bearing veins range between +11.1 and +19.5 ‰, with 25 out of 33 values being in a narrow interval between +14 and +18 ‰ (Fig. 6). Euhedral quartz crystals present as secondary overprint within few of the Variscan quartz veins (e.g., Holderpfad deposit) have δ^{18}O value between +14.6 and +17.8 ‰, consistent with the typical data range for the post-Variscan veins. The range in δ^{18}O values for quartz from post-Variscan veins found in this study compares well with previously reported data from the Schauinsland and Menzenschwand deposits, which are in the range of +15.5 to +19.4 4.‰, and +15.3 to +20.0 ‰, respectively (Weber 1997; Hofmann 1989). In comparison, sedimentary carneol (Silberberg mountain, near Wittichen) and agate from a Permian rhyolite (Feist quarry) have significantly higher δ^{18}O values of +33.4 ‰ and +28.9 ‰, respectively. Combining measured δ^{18}O values of quartz from the fluorite veins with the respective fluid inclusion homogenization temperatures, the calculated $\delta^{18}O_{H2O}$ (using the experimental quartz-water fractionation of Matsuhisa *et al.* 1979) range between –7.5 and +2.1 ‰ (Table 3).

Table 3. Summary of oxygen isotopic data for analysed quartz samples and calculated isotopic composition of the fluid from the post-Variscan hydrothermal veins, of the Schwarzwald.

$\delta^{18}O_{H2O}$ were calculated using the equation of Matsuhisa et al. (1979) and temperatures (T_h) from fluid inclusions.

No.	No. of deposit	Deposit	Sample	Description	δ^{18}O (‰)	T_h (°C)	$\delta^{18}O_{H2O}$ (‰)
1	1	Käfersteige	BTR-29	Milky fine grained quartz	17	130	-0.2
2	1	Käfersteige	BTR-33	Chalcedony	17.6		
3	4	Dorothea	QDC-69	Milky fine grained quartz	18.7		
4	4	Dorothea	BTR 34	Milky fine grained quartz	17.6		
5	11	Friedrich-Christian	GS 135	Euhedral crystals	16.4	110	-3.0
6	11	Friedrich-Christian	GS 135	Coarse grained vein quartz	14.4	110	-5.0
7	11	Friedrich-Christian	GS 119	Qtz-pseudomorph (barite)	17.8		
8	11	Friedrich-Christian	GS 131	Greenish chert	17.1		
9	11	Friedrich-Christian	GS 131	Euhedral crystals	17.2		
10	11	Friedrich-Christian	GS 123	Quartz from gneiss-host	12.5		
11	12	Sophia, Wittichen	484	Euhedral crystals	17.6		
12	12	Sophia, Wittichen	WSB-26	Euhedral crystals	19.2		
13	12	Sophia, Wittichen	WSB-13	Smoky quartz	19.5	80	-4.6
14	13	Johannes, Wittichen	WJB-2	Fine grained vein quartz	17.2		
15	13	Johannes, Wittichen	WJB-17	Euhedral crystals	17.9	85	-5.3
16	14	Neuglück, Wittichen	BTR-37	Euhedral crystals	19	105	-1.2

No.	No. of deposit	Deposit	Sample	Description	$\delta^{18}O$ (‰)	T_h (°C)	$\delta^{18}O_{H2O}$ (‰)
17	19	Hilfe Gottes	PHG-153	Euhedral crystals	11.1		
18	19	Hilfe Gottes	PHG-134	Greenish, dense quartz vein in granite	14.5		
19	19	Hilfe Gottes	PHG-190	Chert	16.4		
20	27	Segen Gottes	BTR-47-II	Late stage quartz veinlet	14.1	147	-1.5
21	28	Artenberg	BTR-48	Coarse grained vein quartz	12.1		
22	28	Artenberg	XSA-15	Euhedral crystals	16.9	87	-5.5
23	31	Wenzel	OWF-111	Single grains in barite	14.3		
24	31	Wenzel	OWF-12	Euhedral crystals	17.6		
25	36	Badenweiler	BTR-39	Milky fine grained quartz	16.4	162	2.1
26	36	Badenweiler	BTR-34	Dense, milky quartz	17.6		
27	40	Teufelsgrund	BTR-6	Quartz druse, crystal	13.9	151	-1.4
28	40	Teufelsgrund	BTR-6	Blue chalcedony	14.7	151	-0.6
29	40	Teufelsgrund	BTR-7	Late-quartz, euhedral crystals	14.7	127	-2.8
30	42	Baumhalde	GS 71	Veinlet with euhedral crystals	11.8	154	-3.2
31	42	Baumhalde	GS 72	Fine grained vein quartz	14.7		
32	42	Baumhalde	GS 76	Chalcedony	13.7		
33	43	Brandenberg	GS 111	Quartz-pseudomorph (barite)	12.5		
34	43	Brandenberg	GS 99	Fine grained vein quartz	13.4	127	-4.1
35	43	Brandenberg	GS 91	Chalcedony	13.8	130	-3.4
36	43	Brandenberg	GS 91	Chalcedony	15	130	-2.2
37	43	Brandenberg	GS 91	Euhedral crystals	15.3	130	-1.9
38	43	Brandenberg	GS 91	Coarse grained vein quartz	13.9	130	-3.3
39	43	Brandenberg	GS 91	Euhedral crystals	13.5	130	-3.7
40	43	Brandenberg	GS 103	Quartz gneiss-host; 4 cm from vein	9.7		
41	47	Herrmann	GS 67	Coarse grained vein quartz	14.4		
42	47	Herrmann	GS 70	Coarse grained vein quartz	14.6		
43	47	Herrmann	GS 68	Euhedral crystals	14.9		
44	53	Schwarzwaldsegen	GS 29c	Euhedral crystals	17.6		
45	54	Neue Hoffnung	GS 35	Euhedral crystals	11.9		
46	54	Neue Hoffnung	GS 34	Quartz-pseudomorph (barite)	17.1		
47	56	Brenden	GS 15	Veinlet in quartz-pseudomorph barite	14.7	95	-6.6

No.	No. of deposit	Deposit	Sample	Description	$\delta^{18}O$ (‰)	T_h (°C)	$\delta^{18}O_{H2O}$ (‰)
48	56	Brenden	GS 15	Quartz-pseudomorph (barite)	13.8	95	-7.5
49	56	Brenden	GS 15	Quartz-pseudomorph (barite)	15.4	95	-5.9
50	56	Brenden	GS 4	Euhedral crystals	15.7		
51	57	Igelschlatt	GS 42	Quartz-pseudomorph (barite)	16.3		
52	57	Igelschlatt	GS 37	Purple quartz	16.8	125	-1.0
53	57	Igelschlatt	GS 37	Quartz granite-host; 1cm from vein	10.8	125	-7.0
54	57	Igelschlatt	GS 37	Quartz granite-host; 6 cm from vein	10.7	125	-7.1
55	57	Igelschlatt	GS 41	Quartz granite-host; 1cm from vein	10.5		
56	57	Igelschlatt	GS 41	Quartz granite-host; 8 cm from vein	10.9		
57	57	Igelschlatt	GS 41	Coarse grained vein quartz	13.7		
58	62	Sulzburg	SW-25a	Euhedral crystals	18.2	120	-0.1
59	62	Sulzburg	SW-25M	Dense, milky quartz	16.4	124	-1.5
60	64	Neubulach	919	Euhedral crystals	16.8		
61	64	Neubulach	BTR-32	Euhedral crystals	16.9	114	-2.1
62	65	Michael im Weiler	566	Bluish, dense quartz	18		
63	65	Michael im Weiler	GMW-121	Smoky quartz	16.3	110	-3.1
64	66	Geigeshalde	TGH-30	Euhedral crystals	15.8		
65	67	Schauinsland	BTR-40	Euhedral crystals	14.4	113	-4.7
66	69	Menzenschwand	GMS 03	Euhedral crystals	19		
67	69	Menzenschwand	GMS 07	Euhedral crystals	20.9		
68	69	Menzenschwand	GMS 08	Reddish chalcedony	16.9		
69	86	Silbergründle	SW-24	Euhedral crystals	16.2	128	-1.2
70	87	Königswart	SW-23	Euhedral crystals	17.1	116	-1.6
71	88	Silberbreunnle	BTR-31	Quartz-pseudomorph (barite)	16.5		
72	88	Silberbreunnle	YSB-195	Euhedral crystals	14.2		
73	88	Silberbreunnle	BTR-31	Chalcedony	14.6		
74	88	Silberbreunnle	BTR-31	Coarse grained vein quartz	15.7	132	-1.3
75	88	Silberbreunnle	YSB-235	Euhedral crystals	16.6		
76	88	Silberbreunnle	BTR-31	Bluish chalcedony	17.2		
77	88	Silberbreunnle	YSB-195	Bluish, dense quartz	18.2		
78	88	Silberbreunnle	BTR-31	Yellow chalcedony	16.5		
79	89	Lorenz	BTR-24	Euhedral crystals	15.9		
80	89	Lorenz	BTR-36	Euhedral crystals	17		

No.	No. of deposit	Deposit	Sample	Description	$\delta^{18}O$ (‰)	T_h (°C)	$\delta^{18}O_{H2O}$ (‰)
81	q-4	Ludwig/Adlersbach*	GS 160	Dense milky quartz	18.8		
82	q-4	Ludwig/Adlersbach*	GS 161	Dense milky quartz	15.1		
83	q-4	Ludwig/Adlersbach*	GS 162	Dense milky quartz	18.4		
84	q-13	Holderpfad **	GS 208	Euhedral crystals	17.8	102	-2.6
85		Silberberg, Wittichen	SW-01	Sedimentary carneol	33.4		
86		Steinbruch Feist	SW-15	Secondary agate from rhyolite	28.9		

* The Variscan veins were overprinted by post-Variscan hydrothermal.
** Late druse on the Variscan vein.

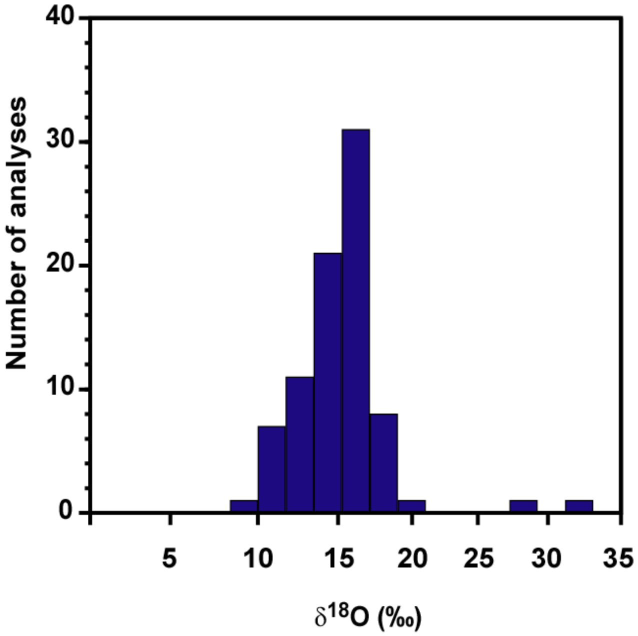

Fig. 6. Histogram showing the ranges of measured $\delta^{18}O_{SMOW}$ for quartz from the post-Variscan hydrothermal veins, in the Schwarzwald.

4.2 Oxygen, hydrogen and carbon isotope systematics of fluid inclusions

Oxygen, hydrogen and carbon isotope compositions of directly extracted fluid inclusion water from fluorites are listed in Table 4. The $\delta^{18}O$ values of fluid inclusion water range from –11.6 to –3.0 ‰ (with most data lying between –6 and –3 ‰), which is very consistent with the $\delta^{18}O_{H2O}$ values calculated from the measured $\delta^{18}O$ of vein quartz and fluid inclusion homogenization temperatures in the same samples (Table 4; Fig. 7). Water yields and the δD values of inclusion fluids from hydrothermal fluorite, calcite and quartz samples are shown in Table 4 and Figure 7. The δD values for water extracted from fluid inclusions in fluorites have a relatively narrow range between –13 and –12 ‰. In comparison, fluid inclusion water from quartz samples generally has more variable and more negative δD values between –63 and +9 ‰, with 7 out of 12 values lying between –63 and –32 ‰. The only exception is shown by a sample from the Neubulach deposit, which has a much higher δD value of +54 ‰. The δD values of fluid inclusion water extracted from primary calcite samples range between –26 and –15 ‰, very similar to the data from primary fluorite. In contrast, late calcite samples have significantly heavier δD values in the range between –5 and +70 ‰ (Table 4). The carbon isotope data of fluid inclusion gas (mainly CO_2) show considerable variation, with $\delta^{13}C$ values between –21.4 and –6.7 ‰. The heaviest value of –6.7 ‰ was obtained from a late stage fluorite sample from the Teufelsgrund deposit.

5. Discussion

5.1Pressure-temperature conditions of post-Variscan mineralization

The results of the integrated fluid inclusion and stable isotope studies of the post-Variscan veins allow a reconstruction of the pressure-temperature conditions prevalent during formation. Combining the measured $\delta^{18}O$ data of quartz and directly extracted fluid inclusion water for pairs of texturally coexisting quartz and fluorite, the equilibrium temperatures have been calculated. Knowing the trapping temperatures of the fluid inclusions, the corresponding pressure is then calculated from the intersection with the respective isochores of the fluid inclusions, which establishes the P-T conditions of vein formation (Fig. 8). It is important to note that fluid inclusion petrography and the microthemometric data demonstrate the contemporaneous formation of texturally coexisting quartz-fluorite pairs. Figure 9 shows a hand specimen from the Brandenberg deposit with histograms of final ice melting temperatures of fluid inclusions in quartz and fluorite, which demonstrates that both minerals were apparently precipitated from the same hydrothermal fluid. Oxygen isotope equilibrium temperatures between bulk quartz and the hydrothermal fluid from fluid inclusions were calculated after Matsuhisa *et al*. (1979), and the corresponding isochores were calculated after Brown & Hageman (1995). The results and the input parameters for the calculation of the isochores are given in Table 5. In order to determine the error interval associated with our calculations, reasonable error ranges of the measured fluid inclusion homogenization temperatures (± 5°C) and the calculated $\delta^{18}O$ equilibrium temperatures (± 5°C, corresponding to approximately ± 0.5 ‰ in $\delta^{18}O$) have been considered. The calculated formation pressures are in the range of 260-610 bar (Fig. 8 and Table 5), with the error interval being on the order of ± 125 bar

Table 4. Summary of stable isotope data for post-Variscan ore forming hydrothermal fluids in the Schwarzwald.

Locality	*No. of deposits*	*Sample ID*	*Mineral*	*H_2O content*	*H_2O*		*CO_2*
					$\delta^{18}O$	δD	$\delta^{13}C$
					(‰ VSMOW)		(‰ VPDB)
Artenberg	28	BTR-35	Fluorite	0.019	-11.6		-10.2
Artenberg	28	BTR-1	Calcite	0.032		-24	
Artenberg	28	BTR-13	Calcite-Late	0.192		-22	
Badenweiler	36	BTR-39	Quartz	0.085		-40	
Baumhalde	42	GS-71	Quartz	0.066		-38	
Brandenberg	43	111	Fluorite				-7.5
Brandenberg	43	GS-91	Quartz	0.033		-9	
Brenden	56	24	Fluorite	0.161	-5.8	-11	-18.3
Brenden	56	GS-4	Quartz	0.035		9	
Dorothea	4	BTR-14	Fluorite	0.068	-3.3		-21.3
Drey	25	151	Fluorite	0.057	-7.4		-15.6
Friedrich Christian	11	FCH-1	Fluorite	0.025	-5.4	-12	-21.4
				0.057	-3.0		-20.9
Friedrich Christian	11	FCH-2	Fluorite	0.02	-2.6	-12	-19.5
Friedrich Christian	11	GS-119	Quartz-Late	0.117		-62	
Friedrich Christian	11	GS-131	Quartz	0.068		-63	
Friedrich Christian	11	38 Cc-I	Calcite	0.059		-26	
Gottes		53	Calcite	0.343		-25	
Igelschlat	57	GS-37	Quartz	0.044		-47	
Igelschlatt	57	37	Fluorite	0.153	-6.2		-11.8
Johannes Wittichen	13	WJB-2	Fluorite	0.11	-5.6	-12	-19.2
Johannes Wittichen	13	WJB-17/4	Quartz	0.158		-36	
Käfersteige	1	BTR-28	Fluorite	0.142	-5.4		-16.4
Michael Weiler	65	GMW102	Quartz	0.055		-28	
Neu Bergmännisch Glück	22	814	Fluorite	0.1	-3.8		-17.8
Neubulach	64	815	Quartz	0.056		53	
Schauinsland	67	17	Calcite	0.094		-25	
Schauinsland	67	446	Quartz	0.037		-22	
Silberbreunnle	88	BTR-31	Quartz	0.049		-32	
Sophia Wittichen	12	BTR-50	Fluorite	0.091	-5.6		-9.2
Sophia Wittichen	12	198	Calcite-Late	0.035		70	

Locality	*No. of deposits*	*Sample ID*	*Mineral*	*H_2O content*	*H_2O*		*CO_2*
					δ^{18}O	δD	δ^{13}C
					(‰ VSMOW)		(‰ VPDB)
Teufelsgrund	40	BTR-7	Fluorite	0.105	-6.0		-11.5
Teufelsgrund	40	BTR-9	Fluorite-Late	0.096	-9		-6.7
Teufelsgrund	40	BTR-8	Calcite-Late	0.052		-4	
Tunnelbau Hausach		HTB-13	Calcite-Late	0.036		48	
Wenzel	31	BTR-42	Calcite	0.166		-15	

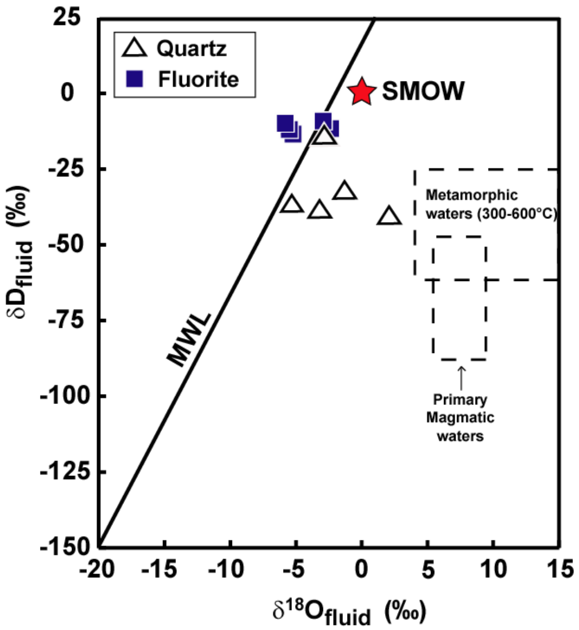

Fig. 7. Fluid δD and δ^{18}O characteristics of post-Variscan hydrothermal veins, along with the field of estimated isotopic compositions for primary magmatic and metamorphic fluids (Sheppard 1986). δ$^{18}O_{fluid}$ for fluorites were measured directly from fluid inclusion water, whereas δ$^{18}O_{fluid}$ for quartz were calculated using equation of Matsuhisa *et al*. (1979).

.

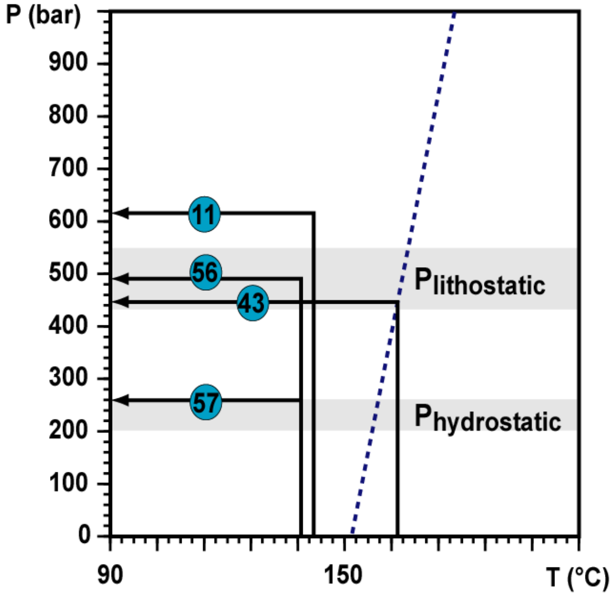

Fig. 8. P-T diagramm with conditions of crystallisation of four deposits (see map for locations). Pressure was calculated by intersecting isotope equilibrium temperatures with isochores (dot line as example)

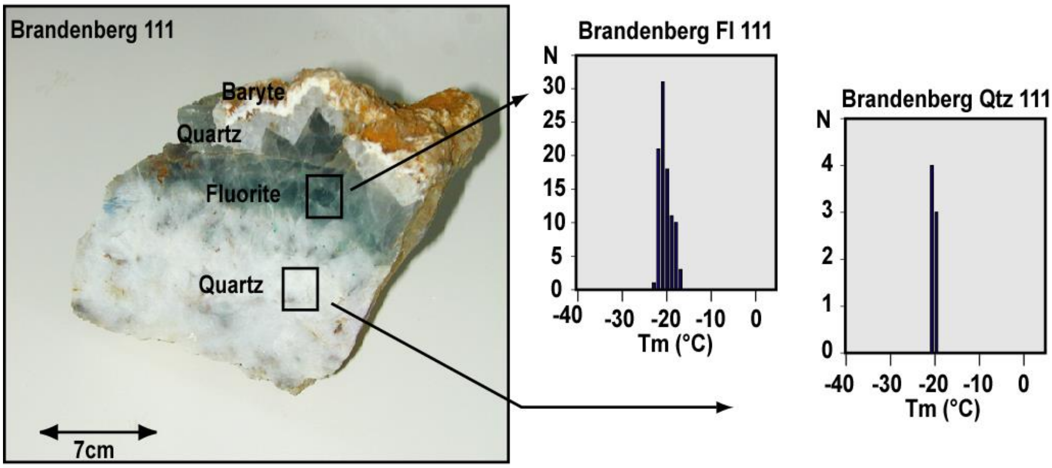

Fig. 9. Cogenetic quartz and fluorite in sample GS-111 with histograms of fluid inclusion melting temperatures in both minerals.

Table 5. Temperature and pressure of formation from □^{18}O ratios and microthermometric data

Locality	Sample ID	$\delta^{18}O$ Quartz (V-SMOW)	$\delta^{18}O$ Fluid (V-SMOW)	Tm (°C)	Th (°C)	$T_{formation}$ (°C)	$P_{formation}$ (bar)
Brandenberg	GS 111	12.5	-1.0	-20	165	173	450
Brenden	GS 24/GS 15	13.8	-3.3	-20	135	132	490
Friedrich-Christian	GS 135	14.3	-2.3	-23	110	137	610
Igelschlatt	GS 37	16.8	-0.2	-22	135	133	260

The sedimentary overburden in the area where the deposits formed prior to the subsidence of the Rheingraben structure can be reconstructed from the regional geology (Geyer & Gwinner 1986) and lithostatic and hydrostatic pressure conditions can be calculated from the barometric equation. For example, the Friedrich-Christian deposit was covered by approximately 1800-2000 m of basement rocks and sediments. With assumed rock and fluid densities of 2.7 and 1.2 g/cm^3 respectively, one can estimate that the hydrostatic pressure should have been around 220 bar and the lithostatic regime around 500 bar (shaded areas in Fig. 8). Comparison of the vein formation pressures determined from fluid inclusion and oxygen isotope data with the litho- and hydrostatic pressures reconstructed from geological constraints shows that the actual pressure conditions apparently varied between lithostatic and hydrostatic pressure conditions.

5.2 Isotopic composition of the post-Variscan hydrothermal fluids

The oxygen isotopic composition of the hydrothermal fluids has been calculated from the measured range in isotopic compositions of quartz within distinct veins and the corresponding pressure corrected fluid inclusion temperatures (Table 4). Resulting equilibrium $\delta^{18}O_{H2O}$ values are within a relatively narrow range of –7.5 to +2.1 ‰. This data range is very consistesnt with the measured $\delta^{18}O_{H2O}$ values (–11.6 to –3.0 ‰) of water directly extracted from fluorite-hosted fluid inclusions. Consequently, the initial $\delta^{18}O$ values of the primary hydrothermal fluids are estimated to be in the range between –10 and 0 ‰. The $\delta^{18}O$ values of the surface-derived meteoric waters can vary along the meteoric water line from 0 ‰ to negative values. Integrating $\delta^{18}O$ data of vein quartz, fluid inclusion homogenization temperatures, and calculated and measured fluid isotopic compositions, all available information points to formation of the post-Variscan vein deposits from saline brines with quite homogeneous geochemical characteristics. The δD (–10 to –60 ‰) and $\delta^{18}O$ (–11.6 to –3.0 ‰) values of fluid inclusion water directly extracted from the vein minerals ($\delta^{18}O$ from fluorite, δD from fluorite, quartz and calcite) are well within the range typical for meteoric water. The deep saline brine is most likely of meteoric or seawater origin (Behr & Gerler 1987; Von Gehlen 1987; Hofmann 1989; German *et al.* 1994; Werner *et al.* 2000; 2002), but was extensively modified through water-rock reactions in the crystalline basement. During high-temperature water-rock interaction with crystalline rocks, the $\delta^{18}O$ of water is generally shifted towards higher values (Taylor 1997). The oxygen data indicate that the hydrothermal fluids have partly exchanged oxygen through progressive fluid-rock interaction in the crystalline basement (Fig. 11). Considering the trends of both $\delta^{18}O$ and δD data of the post-Variscan hydrothermal veins, it appears that the meteoric contribution to the isotopic budget is certainly dominant. The oxygen isotope signature, however, was compositionally modified during fluid ascent and interaction with the surrounding rocks. Schwinn *et al.* (2006) have applied both closed- and open-system scenarios (Taylor 1977; 1997) to model the isotopic exchange between water of meteoric origin (with $\delta^{18}O$ between –5 and 0 ‰) and typical granites of the Schwarzwald area having average primary $\delta^{18}O$ values of 10 ‰ (Hoefs & Emmermann 1983; Simon & Hoefs 1987). The resulting $\delta^{18}O$ values of the deep saline brine are in the range between –1.2 and 5.3 ‰ for geologically reasonable water/rock ratios between 0.01 and 1.0 and an exchange temperature of 300°C.

The $\delta^{13}C$ values of directly extracted fluid inclusion gas, which are in the range between –21.4 and –6.7 ‰, are systematically lower than the values for primary hydrothermal calcites from the post-Variscan veins, which are between –12.0 and –3.0 ‰ (Schwinn *et al.* 2006). This difference cannot be explained through equilibrium fractionation between calcite and dissolved inorganic carbon species in the fluids in the temperature interval 150-200°C. Applying equilibrium fractionation factors for both CO_2 (aq) and HCO_3^- (Ohmoto & Goldhaber 1997), which are most likely the predominant dissolved carbon species in the fluids, results in calculated $\Delta_{CAL\text{-}CO2}$ of 0.9 to –0.7 ‰, and $\Delta_{CAL\text{-}HCO3}$ of 1.1 to 2.0 ‰. This is much smaller than the observed difference in carbon isotope composition between the bulk fluid inclusion gas and the hydrothermal calcites. Although the dominant volatile component in the fluid inclusions is CO_2 as shown by the Raman spectra, it appears probable that minor amounts of a second volatile component with significantly more negative $\delta^{13}C$ values contribute to the bulk carbon isotope composition of the fluid inclusion gas. A likely candidate for this component is gaseous CH_4, which has been found at detectable concentrations in fluid inclusions from the Schauinsland deposits (Werner *et al.* 2002). Based on mass balance considerations, even small amounts of CH_4 with very negative $\delta^{13}C$ values could shift the bulk carbon isotopic composition of the fluid inclusions towards more negative values. This, in turn, would have no impact on the $\delta^{13}C$ values of the hydrothermal calcites, because in comparatively rapid processes such as fluid migration and fluid mixing CH_4 would not equilibrate with oxidized aqueous carbon species due to kinetic restrictions (Ohmoto & Goldhaber 1997).

5.3 The post-Variscan fluid system

Isotopic characteristics well comparable to the post-Variscan fluid system in the Schwarzwald area have been reported from other hydrothermal fluids originating in crystalline basement rocks. Fluids sampled during pumping tests of the KTB pilot hole have δD and $\delta^{18}O$ values in the range between –32 and –27 ‰ and between –5.8 to –5.7 ‰, respectively (Lodemann *et al.* 1997). Simon & Hoefs (1991) postulated a direct relationship between the fluids responsible for vein mineralization visible throughout the KTB drillcore profile and the fluids encountered at 4000 m depth at the KTB site. Based on a comprehensive fluid inclusion study, Behr *et al.* (1993a, 1994) concluded that fluids with Ca-Na-Cl characteristics are compositionally very similar to the present fracture fluids, indicating a common primary fluid source. Below about 6000 m, Ca-Na-Cl fluid inclusions with homogenization temperatures up to 250°C dominate and represent a young fluid system, probably of late Cretaceous age (Behr *et al.* 1994).

Our extensive fluid inclusion study of hydrothermal veins demonstrates that post-

Variscan fluids originate from deep highly saline $NaCl-CaCl_2-H_2O$ brines that mixed with low salinity meteoric water. The temperature of the $NaCl-CaCl_2$ fluid prior to mixing cannot be directly determined by means of fluid inclusions. Based on isotope temperature calculations from sulfide-sulfate equilibria and paleogeothermal considerations, the aquifer paleotemperatures of the deep saline brine are estimated at 300-350°C (Schwinn *et al*. 2006).

Integrating all available datasets from the post-Variscan hydrothermal veins in the Schwarzwald district (including the comprehensive fluid inclusion and stable isotope data from the present study), the post-Variscan mineralization process is best explained through mixing of a deep saline brine with surface-derived meteoric waters.

6. Conclusions

By combining stable isotope and fluid inclusion techniques it has been possible to decipher the complexities of prolonged hydrothermal activity in the Schwarzwald ore district, SW Germany.

Fluid belongs to the $NaCl-CaCl_2-H_2O$ type, is generally of higher salinity (20-25 wt.% eqv. NaCl) and lower temperature (100-160°C). Late-stage mineral generations in the post-Variscan veins host secondary fluid inclusions of lower salinity, but with similar homogenization temperatures. Both the fluid inclusion and oxygen and hydrogen isotope systematics suggest that the post-Variscan fluid originated from large-scaling mixing of a deep-sourced saline brine with surface-derived meteoric water. It was responsible for the formation of Pb±Zn±Cu-barite-fluorite veins.

By integrating all data from this study with additional isotopic datasets from previous work, a consistent model for post-Variscan hydrothermal mineralization can be developed. This model envisages upward circulation of a 300-350°C hot saline brine ($NaCl-CaCl_2-H_2O$) through strike-slip fault systems. During periods of increased tectonic activity, efficient mixing of this brine with low-temperature surface-derived meteoric water was facilitated. The mixing process resulted in precipitation of the major fluorite-barite-quartz generation of the post-Variscan veins. This fluid system was active over an area of 120 by 40 km and over at least 100 Ma.

References

Baatartsogt B, Schwinn G, Wagner T, Taubald H, Beitter T, Markl G (2006) Contracting paleofluid systems in the continental basement: fluid inclusion and stable isotope study of hydrothermal vein mineralization, Schwarzwald district, Germany. *Geofluids,* 7, 123-147.

Behr HJ, Horn EE (1984a) Quarzbildung und Verkieselungsprozesse in den Karbonatkomplexen des Rheinischen Schiefergebirges. *In: Postvaristische Gangmineralisationen in Mitteleuropa. G.D.M.B. (Ges. Dtsch. Mitallhütten-Bergleute)*, **41**, 27-45.

Behr HJ, Horn EE (1984b) Unterscheidungskriterien für Mineralisationen des varistischen und postvaristischen Zyklus, die aus der Analyse fluider Einschlüsse gewinnbar sind. *In: Postvaristische Gangmineralisationen in Mitteleuropa. G.D.M.B. (Ges. Dtsch. Mitallhütten-Bergleute)*, **41**, 255-269.

Behr HJ, Horn EE, Lüders V, Reutel Chr (1984) Genetische Schlussfolgerung für die Gangmineralisationen des Harzes aus der Untersuchung fluider Einschlüsse. *Fortschr. Mineralogie*, **62**, 18.

Behr HJ, Gerler J (1987) Inclusions of sedimentary brines in post-Variscan mineralizations in the Federal Republic of Germany: A study by Neutron Activation Analysis. *Chemical Geology*, **61**, 65-77.

Bodnar RJ, Vityk MO (1994) Interpretation of microthermometric data for H_2O-NaCl fluid inclusions. *in* Fluid Inclusions in Minerals, Methods and Applications, B. De Vivo and M.

L. Frezzotti, eds., *pub. by Virginia Tech, Blacksburg, VA*, 117-130.

Borisenko AS (1977) Study of the salt composition of solutions in gas-liquid inclusions in minerals by the cryometric method. *Soviet Geoogy and Geophysics,* **18**. 11-19.

Boiron MC, Cathelineau M, Banks DA, Fourcade S, Vallance J (2003) Mixing of metamorphic and surficial fluids during the uplift of the Hercynian upper crust: consequences for gold deposition. *Chemical Geology*, **194**, 119-141.

Brown PE, Hagemann SG (1995) Fluid inclusion data reduction and interpretation using MacFlinCor on the Macintosh. XIII ECROFI Symposium, Barcelona, *Boletin de la Sociedad Espaola de Mineralogia*, **18-1**, 32-33.

Burke EAJ (2000) Raman microspectrometry of fluid inclusions. *Lithos*, **55**, 139-158.

Canals A, Cardellach E (1993) Strontium and sulfur isotope geochemistry of low-temperature barite-fluorite veins of the Catalonian Coastal Ranges (NE Spain): a fluid mixing model and age constraints. *Chemical Geology*, **104**, 269-280.

Charef A, Sheppard SMF (1988) The Malines Cambrian carbonate-shale-hosted Pb-Zn deposit, France: thermometric and isotopic (H,O) evidence for pulsating hydrothermal mineralization. *Mineralium Deposita*, **23**, 86-95.

Clauer N, O'Neil JR, Furlan S (1995) Clay minerals as record of temperature conditions and duration of thermal anomalies in the Paris basin, France. *Clays and Clay Minerals*, **30**, 1-13.

Craig H (1957) Isotopic standards for carbon and oxygen and correction factors for mass spectrometric analysis of carbon dioxide. *Geochimica et Cosmochimica Acta*, **12,** 133-149.

Craig H (1961) Standards for reporting concentrations of deuterium and oxygen 18 in natural waters. *Science*, **133**, 1833-1834.

Craig H (1961) Isotopic variations in meteoric waters. *Science*, **133,** 1702-1703.

Davis DW, Lowenstein TK, Spencer RJ (1990) Melting behaviour of fluid inclusions in laboratory-grown halite crystals in the systems $NaCl-H_2O$, $NaCl-KCl-H_2O$, $NaCl-MgCl_2-H_2O$, and $NaCl-CaCl_2-H_2O$. *Geochimica et Cosmochimica Acta*, **54**, 591-601.

Franzke HJ, Ahrendt H, Kurz S, Wemmer K (1996) K-Ar Datierungen von Illiten aus Kataklasiten der Floßbergstörung im südöstlichen Thüringer Wald und ihre geologische Interpretation. *Zeitschrift für geologische Wissenschaften*, **24**, 441-456.

Frape SK, Fritz P (1987) Geochemical trends for groundwaters from the Canadian Shield. *In Saline Water and Gases in Crystalline rocks* (eds P. Fritz and S.K. Frape). *Geol. Assoc. Canad. Spec. Pap*. **33**, 19-38.

Friedman I (1953) Deuterium content of natural water and other substances. *Geochimica et Cosmochimica Acta*, **4**, 89-103.

Fritz P, Frape SK (1982) Saline groundwaters in the Canadian Shield. A first overview. *Chem. Geol*. **36**, 179-190.

Hein UF (1993) Synmetamorphic Variscan siderite mineralization of the Rhenish Massif, Central Europe. *Mineralogical Magazine*, **57**, 451-467.

Hoefs J, Emmermann R (1983) The Oxygen Isotope Compostion of Hercynian Granites and Pre- Hercynian Gneisses from the Schwarzwald, SW Germany. *Contributions to Mineralogy and Petrology*, **83**, 320-329.

Lippolt HJ, Kirsch H (1994) Isotopic Investigation of Post-Variscan Plagioclase Sericitization in the Schwarzwald Gneiss Massif. *Chemie der Erde*, **54**, 179-198.

Lippolt HJ, Werner O (1994) Die Genetische Aussage von Blei- Isotopen- Verhältnissen in Bleiglanzen des Bergbaureviers Freiamt-Sexau, Mittlerer Schwarzwald. In: D.H. Storch and W. Werner (Editors), Die Erz- und Mineralgänge im alten Bergbaurevier "Freiamt- Sexau", Mittlerer Schwarzwald. *Abhandlungen des Geologischen Landesamtes Baden-Württemberg,* **14**, 191-205.

Lodemann M, Fritz P, Wolf M, Ivanovich M, Hansen BT, Nolte E (1997) On the origin of saline fluids in the KTB (continental deep drilling project of Germany). *Applied Geochemistry*, **12**, 831-849.

Matsuhisa Y, Goldsmith HJR, Clayton RN (1979) Oxygen isotopic fractionation in the system quartz-albite-anorthite-water. *Geochimica et Cosmochimica Acta,* **43**, 1131-1140.

Meshik AP, Lippolt HJ, Dymkov YM (2000) Xenon geochronology of Schwarzwald pitchblendes. *Mineralium Deposita*, **35**, 190-205.

Metz R, Richter M, Schürenberg H (1957) Die Blei-Zink-Erzgänge des Schwarzwaldes. *Beihefte Geologisches Jahrbuch*, **29**, 1-277.

Meyer M, Brockamp O, Clauer N, Renk A, Zuther M (2000) Further evidence for a Jurassic mineralizing event in central Europe. K-Ar dating of geothermal alteration an fluid inclusion systematics in wall rocks of the Käferteige fluorite vein deposit in the northern Black Forest, Germany. *Mineralium Deposita*, **35**, 754-761.

Munoz M, Premo WR, Courjault-Rade (2005) Sm-Nd dating of fluorite from the worldclass Montroc fluorite deposit, southern Massif Central, France. *Mineralium Deposita*, **39**, 970-975.

Nurmi PA, Kukkonen IT, Lahermo PW (1988) Geochemistry and origin of saline groundwaters in the Fennoscandian Shield. *Appl. Geochem*. **3**, 185-203.

Ohmoto H. Goldhaber MB (1997) Sulfur and carbon isotopes. In: *Geochemistry of Hydrothermal Ore Deposits* (ed. H.L. Barnes), **3rd ed**., Wiley, New York, 517-611.

Ritter J (1995) Genese der Mineralistation Herrmanngang im Albtalgranit, SE-Schwarzwald und Wechselwirkungen mit dem Nebengestein. In: Puchelt (Editor), *Karlsruher Geochemische Hefte*, **8**, 1-132.

Roedder E (1984) Fluid inclusions. *Reviews Mineralogy*, **12**, 644.

Roedder E (1979) Fluid Inclusions as Samples of Ore Fluids. Geochemistry of Hydrothermal Ore Deposits. *Wiley*. 684.

Rumble D III, Hoering TC (1994) Analysis of oxygen and sulfur isotope ratios in oxide and sulfide minerals by spot heating with a carbon dioxide laser in a fluorine atmosphere. *Account of Chemical Research,* **27**, 237-241.

Schwinn G, Wagner T, Baldorj B, Markl G (in press) Quantification of mixing processes in ore-forming hydrothermal systems by combination of stable isotope and fluid inclusion analyses. *Geochimica et Cosmochimica Acta,* **70, 965-982**

Segev A, Halicz L, Lang B, Steinitz G (1991) K-Ar dating of manganese minerals from the Eisenbach region, Black Forest, southwest Germany. *Schweizerische Mineralogische und Petrogaphische. Mitteilungen,* **71**, 101-114.

Simon K, Hoefs J (1993) O, H, C isotope study of rocks from the KTB pilot hole: crustal profile and constraints on fluid evolution. *Contributions to Mineralogy and Petrol*ogy, **114**, 42-52.

Simon K (2001) Does δD from fluid inclusion quartz reflect the original hydrothermal fluid? *Chemical Geology*, **177**, 483-495.

Stober I, Bucher K (1999) Deep groundwater in the crystalline basement of the Black Forest region. *Applied Geochemistry*, **14**, 237-254.

Taylor HP Jr (1974) The application of oxygen and hydrogen isotope studies to problems of hydrothermal alteration and ore deposition. *Economic Geology*, **69**, 843-883.

Taylor HP Jr (1977) Water/rock interactions and the origin of H_2O in granitic batholiths. *Journal of the Geological Society London*, **133**, 509-558.

Taylor HP Jr (1979) Oxygen and hydrogen isotope relationships in hydrothermal mineral deposits. In: *Geochemistry of hydrothermal ore deposits,* **2nd Ed.** *(ed. Barnes HL)*, 236-277.

Von Gehlen (1987) Formation of Pb-Zn-F-Ba-mineralizations in SW-Germany: a status report. *Fortschr. Miner.,* **65**, 87-113, Stuttgart.

Von Gehlen (1989) Ore and Mineral Deposits of the Schwarzwald. In: R. Emmermann and J. Wohlenberg (Editors), *The German Continental Deep Drilling Program, Springer Verlag*, 276-295.

Vovk IF, Vysotskii VI (1982) Isotopic composition and geochemical characteristics of subsurface waters of the Krivoi Rog Basin as indicators of their interrelation and origin. *Water Res*. **9**, 15-21.

Werner W, Dennert V (2004) Lagestätten und Bergbau im Schwarzwald. Freiburg.